



Received December 18, 2017, accepted January 25, 2018, date of publication January 30, 2018, date of current version March 13, 2018.

Digital Object Identifier 10.1109/ACCESS.2018.2799905

A Multiscale Sparse Array of Spatially Spread Electromagnetic-Vector-Sensors for Direction Finding and Polarization Estimation

MINGLEI YANG¹ , (Member, IEEE), JIN DING¹, BAIXIAO CHEN¹,
AND XIN YUAN² , (Senior Member, IEEE)

¹National Laboratory of Radar Signal Processing, Xidian University, Xi'an 710071, China

²Nokia Bell Labs, Murray Hill, NJ 07974 USA

Corresponding author: Xin Yuan (xyuan@bell-labs.com)

This work was supported in part by the National Natural Science Foundation of China under Grant 61571344, in part by the Foundation of Shanghai Academy of Spaceflight Technology under Grant SAST2016093, and in part by the Fund for Foreign Scholars in University Research and Teaching Programs the 111 Project under Grant B18039.

ABSTRACT In this paper, a multiscale sparse array, which is composed of spatially-spread electromagnetic-vector-sensors (SS-EMVSs), is proposed to estimate the direction-of-arrivals (DOA) and polarizations of multiple sources. The SS-EMVS is composed of three orthogonally oriented but spatially noncollocated dipoles to measure the electric field and three orthogonally oriented but spatially noncollocated loops to measure the magnetic field, simultaneously. In this paper, an array of SS-EMVSs is placed along the y -axis, and this sparse array is composed of two sub-arrays, *i.e.*, the first n_1 SS-EMVSs with inter-sensor spacing D_1 , and the last n_2 SS-EMVSs with inter-sensor spacing D_2 , with $D_2 = mD_1$; $m > 1$ is an integer and D_1 is larger than a half-wavelength of the incident signal. Thereby, a multiscale sparse array is constructed, which is capable of providing high accuracy estimates of DOA and polarizations of multiple sources. The vector-cross-product algorithm is used to obtain the unambiguous but low-accuracy estimations of direction cosines, and the different inter-sensor spacings are used to estimate high-accuracy but ambiguous estimations of direction cosines. Following this, a multiscale disambiguation algorithm is developed to obtain high-accuracy and unambiguous estimations of direction cosines, thus the elevation angles, azimuth angles, as well as the polarization parameters of multiple sources. Simulation results verify the superior performance of the proposed multiscale SS-EMVS array.

INDEX TERMS Sensor arrays, direction-of-arrival (DOA) estimation, polarization estimation, direction finding, sparse array, nested array, electromagnetic-vector-sensor.

I. INTRODUCTION

The electromagnetic-vector-sensor (EMVS) has received extensive attention in array signal processing due to the fact that it can not only provide the direction-of-arrivals (DOA) of the signal, but can also give the polarization information. An electromagnetic vector-sensor usually consists of three orthogonally oriented dipoles to measure the electric field, plus three orthogonally oriented loops to measure the magnetic field of the source [1]. A unique DOA estimation algorithm for the EMVS, the vector-cross-product algorithm, has been proposed in [1] and been advanced in [2] and [3] along with various eigenstructure-based direction-finding schemes [4]–[6]. Unfortunately, the mutual coupling between the EMVS components affects the performance of

the algorithm severely. In 2011, Wong and Yuan [7] proposed a spatially-spread EMVS (SS-EMVS) which consists of six orthogonally oriented but spatially non-collocating dipoles and loops. This SS-EMVS reduces the mutual coupling between antenna components, and the developed algorithm retains the effectiveness of the vector-cross-product algorithm. Following this, a flurry of spatially-spread polarized antenna arrays have been proposed [8]–[14]. Various compositions of sparsely polarized antenna array were proposed in [10] for coherent source direction finding. He and Liu [11] proposed a computationally efficient method for DOA and polarization estimation using arbitrarily spaced EMVSs at unknown locations. In [12], the way of how the four/five spatially non-collocated dipoles/loops suffice for

multi-source azimuth/elevation direction finding and polarization estimation was developed. A nonuniform L-shaped spatially spread loop and dipole array, whose inter-element spacing is greater than a half wavelength was exploited in [13]. In [14], a closed-form solution for DOA estimation using the spatially stretched tripole by adopting a quasi-vector-cross-product based scheme was presented.

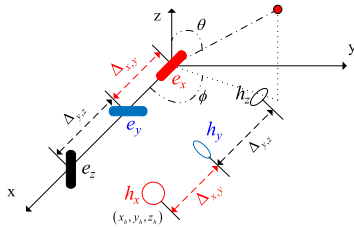


FIGURE 1. Configuration of the SS-EMVS [7].

A. SPATIALLY-SPREAD ELECTROMAGNETIC-VECTOR-SENSOR

Fig. 1 depicts the array configuration for the SS-EMVS proposed in [7]. The three dipoles are placed on a straight line; the three loops are placed on a parallel straight line in an opposite order. In the following, we consider the case that these two lines are parallel to the x -axis in the Cartesian coordinate system with e_x being located at the origin and h_x is located at (x_h, y_h, z_h) .

Considering a far-field source, located at elevation angle $\theta \in [0, \pi]$ and azimuth angle $\phi \in [0, 2\pi)$, with polarization parameters (γ, η) , where γ refers to the auxiliary polarization angle, and η represents the polarization phase difference. The array manifold \mathbf{a} can be characterized by the electric-field vector $\mathbf{e} = [e_x, e_y, e_z]^T$ and the magnetic-field vector $\mathbf{h} = [h_x, h_y, h_z]^T$ by taking account of the inter-dipole/loop spacings $\{\Delta_{x,y}, \Delta_{y,z}\}$,

$$\mathbf{a} = \underbrace{\begin{bmatrix} 1 \\ e^{-j\frac{2\pi}{\lambda} \Delta_{x,y} u} \\ e^{-j\frac{2\pi}{\lambda} (\Delta_{x,y} + \Delta_{y,z}) u} \\ e^{-j\frac{2\pi}{\lambda} (x_h u + y_h v + z_h w)} \\ e^{-j\frac{2\pi}{\lambda} [(x_h u + y_h v + z_h w) - \Delta_{x,y} u]} \\ e^{-j\frac{2\pi}{\lambda} [(x_h u + y_h v + z_h w) - (\Delta_{x,y} + \Delta_{y,z}) u]} \end{bmatrix}}_{\text{def } \xi} \odot \begin{bmatrix} e_x \\ e_y \\ e_z \\ h_x \\ h_y \\ h_z \end{bmatrix}, \quad (1)$$

where

$$\underbrace{\begin{bmatrix} e_x \\ e_y \\ e_z \\ h_x \\ h_y \\ h_z \end{bmatrix}}_{\text{def } \mathbf{a}^o} = \underbrace{\begin{bmatrix} \cos \phi \cos \theta & -\sin \phi \\ \sin \phi \cos \theta & \cos \phi \\ -\sin \theta & 0 \\ -\sin \phi & -\cos \phi \cos \theta \\ \cos \phi & -\sin \phi \cos \theta \\ 0 & \sin \theta \end{bmatrix}}_{\text{def } \Theta(\theta, \phi)} \underbrace{\begin{bmatrix} \sin \gamma e^{j\eta} \\ \cos \gamma \end{bmatrix}}_{\text{def } \beta}, \quad (2)$$

and λ represents the wavelength of the signal, the superscript T is the transposition operator, \odot denotes Hadamard

(element-wise) product, $j = \sqrt{-1}$, and

$$\begin{cases} u = \sin \theta \cos \phi \\ v = \sin \theta \sin \phi \\ w = \cos \theta \end{cases} \quad (3)$$

represents the direction cosines along the x -, y - and z -axis, respectively.

B. SPARSE ARRAYS AND THE COMBINATION WITH VECTOR SENSORS

The DOA estimation accuracy is proportional to the aperture of the array, and therefore an array with a larger aperture is desired. However, due to the phase ambiguity, the spacing between adjacent antennas usually should not be greater than $\lambda/2$. In this way, a large aperture array requires more antennas and thus increasing the cost and also the mutual coupling between antennas. In order to mitigate this limitation, various sparse array configurations and the corresponding DOA estimation algorithms have been proposed. One type of sparse array is constructed by multiple widely separated sub-arrays [15]–[17], and the corresponding rotational invariance technique (ESPRIT)-based algorithms which used the dual-size or multiple invariance within these arrays were developed therein. Another type of sparse array is designed to obtain as many as degree-of-freedom (DOF) to resolve more sources than sensors, such as the minimum-redundancy array [18], the nested array [19] and the co-prime array [20]. Their DOA estimation algorithms focused on using the high order statistic characteristics of the sparse array data to increase the number of DOF, and thereby required a large computational workload. Furthermore, the antenna unit of these sparse arrays is a single polarized antenna, and they cannot measure the polarization information of the source.

Meanwhile, there are some research about the EMVS array and the corresponding parameter estimation algorithms. A distributed signals general model with electromagnetic vector sensor array and the corresponding algorithm based on the generalization MUSIC algorithm were proposed in [21]. Gong et al. [22] studied a new quad-quaternion model established for an electromagnetic vector-sensor array. And a multidimensional algebra-based (DOA) estimation algorithm under this array configuration was proposed. Diao and An [23] proposed a two-dimensional direction finding method using an L-shape EMVS array. These EMVS arrays can provide the DOA and polarization information simultaneously. But these arrays are not sparse, and thus the mutual coupling and the cost cannot be mitigated. Recently, some sparse vector sensor arrays are proposed to overcome the limitations. For example, Han and Nehorai [24] developed a nested vector sensor array and the processing via tensor modeling. He proposed a nested cross dipole array in [25], and Rao et al. [26] proposed a new class of sparse acoustic vector sensor arrays. However, the EMVS unit in the above arrays is not spatially spread, and thus the mutual coupling between the components within a unit is still a concern.

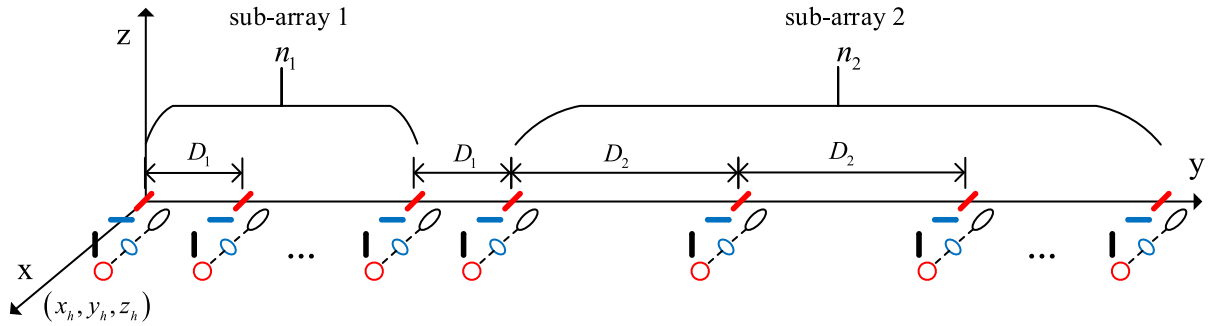


FIGURE 2. The proposed array configuration. The SS-EMVS in Fig. 1 is used as a unit in our multi-scale sparse array which contains two sub-arrays. Every SS-EMVS is placed along the x -axis and the array is extended along y -axis. The inter-sensor (here sensor denoting the SS-EMVS) spacing in sub-array 1 is D_1 and the inter-sensor spacing in sub-array 2 is D_2 , respectively, where $D_2 = mD_1$ and $D_1 \gg \lambda/2$.

C. CONTRIBUTIONS OF THIS WORK

In this paper, we propose a multiscale sparse SS-EMVS array and the corresponding parameter estimation algorithm. The proposed array is a linear sparse array composed of SS-EMVSs which can be divided into two (uniform) sub-arrays with different inter-sensor spacings. Owing to the spatial spread of the SS-EMVS and different inter-sensor spacings of the two sub-arrays, we can obtain multiscale estimations of target parameters. From a single SS-EMVS, we can obtain an unambiguous but low-accuracy estimation of targets parameters using the vector-cross-product algorithm. In addition, we can obtain two high-accuracy but cyclically ambiguous estimations of desired direction cosine by applying the ESPRIT algorithm to the two sub-arrays, respectively. Following this, we employ a two-order disambiguation method to obtain the final high-accuracy and unambiguous estimations of target directions. Furthermore, we can obtain the corresponding polarization parameters with the help of direction estimations. The proposed array integrates the advantages of sparse array and SS-EMVS in reducing mutual coupling and achieving high accuracy DOA estimation. Since we use the approach of disambiguation instead of virtual ULA as in the nested array, there is no need to utilize the high order statistic characteristics of the sparse array data as shown in [19]. Thus, the proposed algorithm enjoys a low computational workload.

The rest of this paper is organized as follows. Section II presents the proposed array geometry. Section III derives the proposed algorithm for DOA and polarization estimation. Section IV gives the derivation of the Cramér-Rao bound (CRB). In section V, numerical examples are provided to show the effectiveness and advantages of the proposed array and algorithm. Section VI concludes the paper.

II. ARRAY GEOMETRY

Fig. 2 demonstrates the proposed array configuration of the multiscale sparse SS-EMVS array. It can be seen that the unit is an SS-EMVS as shown in Fig. 1 and the six noncollocated dipoles/loops in the SS-EMVS are placed in parallel to the

x -axis. We set the SS-EMVS whose e_x is located at the origin being the reference. The sparse array is composed of two sub-arrays. The first sub-array, which consists of the first n_1 SS-EMVSs (close to the origin in Fig. 2), is placed with inter-sensor spacing $D_1 \gg \lambda/2$. The second sub-array, which consists of the last n_2 SS-EMVSs, is placed with an even larger inter-sensor spacing $D_2 = mD_1$, where m is an integer. Following this, the array manifold of the proposed sparse SS-EMVS array is

$$\mathbf{b} = \begin{bmatrix} 1 \\ e^{-j\frac{2\pi}{\lambda}D_1v} \\ \vdots \\ e^{-j\frac{2\pi}{\lambda}(n_1-1)D_1v} \\ e^{-j\frac{2\pi}{\lambda}n_1D_1v} \\ e^{-j\frac{2\pi}{\lambda}(n_1D_1+D_2)v} \\ \vdots \\ e^{-j\frac{2\pi}{\lambda}[n_1D_1+(n_2-1)D_2]v} \end{bmatrix} \otimes \mathbf{a}, \quad (4)$$

where \otimes denotes the Kronecker product, \mathbf{a} is defined in Eq. (1), and thus $\mathbf{b} \in \mathbb{C}^{6N \times 1}$ with $N = n_1 + n_2$.

In a multiple sources scenario with K incident signals, the received data of the proposed sparse array at time t is

$$\mathbf{x}(t) = \sum_{k=1}^K \mathbf{b}_k s_k(t) + \mathbf{n}(t) = \mathbf{B}\mathbf{s}(t) + \mathbf{n}(t), \quad (5)$$

where $\mathbf{b}_k \in \mathbb{C}^{6N \times 1}$ represents the array manifold of the k -th signal and $\mathbf{B} = [\mathbf{b}_1, \mathbf{b}_2, \dots, \mathbf{b}_K] \in \mathbb{C}^{6N \times K}$. $\mathbf{s}(t) = [s_1(t), s_2(t), \dots, s_K(t)]^T$ denotes the incident signal vector, and $\mathbf{n}(t)$ signifies the additive white noise.

Consider L time snapshots, we can form the received data matrix

$$\mathbf{X} = [\mathbf{x}(t_1), \mathbf{x}(t_2), \dots, \mathbf{x}(t_L)]. \quad (6)$$

And the following step is to estimate the DOA and polarization parameters of the K sources from $\mathbf{X} \in \mathbb{C}^{6N \times L}$, which will be described in detail below.

III. DOA AND POLARIZATION ESTIMATION

The main steps of our algorithm are as follows:

- 1) Estimate the *two sets of high-accuracy but cyclically ambiguous y-axis direction cosine* v by the two sub-arrays using the ESPRIT algorithm [27], respectively. It is worth noting that these two sets of v estimations are paired automatically (see Section III-A).
- 2) Estimate the *unambiguous but low-accuracy y-axis direction cosine* v as well as the *high-accuracy and unambiguous x-axis direction cosine* u from the single SS-EMVS as in [7]. Note that the *unambiguous but low-accuracy* estimates of (u, v) are obtained from the absolute values of the “vector-cross-product” algorithm result, while the *high-accuracy but cyclically ambiguous* estimate of u is from the phase of the “vector-cross-product” algorithm result. Furthermore, the different estimates of u are automatically paired.
- 3) Disambiguate the ambiguous v estimates and calculate the final arriving angles and polarization parameters of the sources.

A. ESPRIT BASED METHOD TO ESTIMATE THE TWO SETS OF HIGH-ACCURACY BUT CYCLICALLY AMBIGUOUS v

The array covariance matrix can be calculated by the maximum likelihood estimation

$$\hat{\mathbf{R}} = \mathbf{X}\mathbf{X}^H, \quad (7)$$

where the superscript H is the Hermitian operator. Following [16], let $\mathbf{E}_s \in \mathbb{C}^{6N \times K}$ be the signal subspace matrix composed of the K eigenvectors corresponding to the K largest eigenvalues of $\hat{\mathbf{R}}$. Therefore, \mathbf{E}_s has the same signal subspace with manifold matrix \mathbf{B} and thus

$$\mathbf{E}_s = \mathbf{B}\mathbf{T}, \quad (8)$$

where \mathbf{T} denotes an unknown $K \times K$ non-singular matrix. Due to the multiple scales of the proposed sparse array, we divide the manifold matrix \mathbf{B} into two parts, *i.e.*, \mathbf{B}_1 and \mathbf{B}_2 , where $\mathbf{B}_1 \in \mathbb{C}^{6n_1 \times K}$ is composed of the top n_1 rows of \mathbf{B} (with inter-sensor spacing D_1), and $\mathbf{B}_2 \in \mathbb{C}^{6n_2 \times K}$ is composed of the bottom n_2 rows of \mathbf{B} (with inter-sensor spacing D_2). In this way, \mathbf{B}_1 and \mathbf{B}_2 are the manifold matrices of the sub-array 1 and sub-array 2, respectively. Similarly, we can divide the signal subspace matrix \mathbf{E}_s into two parts with the same method, *i.e.*, \mathbf{E}_{s_1} and \mathbf{E}_{s_2} , where $\mathbf{E}_{s_1} \in \mathbb{C}^{6n_1 \times K}$ is composed of the top n_1 rows of \mathbf{E}_s , and $\mathbf{E}_{s_2} \in \mathbb{C}^{6n_2 \times K}$ is composed of the bottom n_2 rows of \mathbf{E}_s . Thus, we have

$$\mathbf{E}_{s_1} = \mathbf{B}_1\mathbf{T}, \quad (9)$$

$$\mathbf{E}_{s_2} = \mathbf{B}_2\mathbf{T}. \quad (10)$$

After this, we perform the ESPRIT algorithm to both \mathbf{E}_{s_1} and \mathbf{E}_{s_2} to get the high-accuracy but cyclically ambiguous estimates of v . Let us take \mathbf{E}_{s_1} as an example to demonstrate the derivation. We form the matrix-pencil by the top $(n_1 - 1)$ and bottom $(n_1 - 1)$ SS-EMVSs in the sub-array 1 (with inter-sensor spacing D_1). The manifold matrices corresponding to

these two sets of SS-EMVSs are denoted by $\mathbf{B}_{1,1}$ and $\mathbf{B}_{1,2}$, respectively. Utilizing the spatial invariance property between $\mathbf{B}_{1,1}$ and $\mathbf{B}_{1,2}$, we have

$$\mathbf{b}_{1,2}(k) = \mathbf{b}_{1,1}(k)e^{-j\frac{2\pi}{\lambda}D_1v_k}, \quad \forall k \in 1, \dots, K, \quad (11)$$

where $\mathbf{b}_{1,1}(k)$ is the k -th column of $\mathbf{B}_{1,1}$. Specifically, $\mathbf{b}_{1,1}(k) = [\mathbf{a}_k, e^{-j\frac{2\pi}{\lambda}D_1v_k}\mathbf{a}_k, \dots, e^{-j(n_1-2)\frac{2\pi}{\lambda}D_1v_k}\mathbf{a}_k]$, and \mathbf{a}_k denotes the array manifold of k -th source at the reference SS-EMVS. Similarly, $\mathbf{b}_{1,2}(k) = [e^{-j\frac{2\pi}{\lambda}D_1v_k}\mathbf{a}_k, \dots, e^{-j(n_1-1)\frac{2\pi}{\lambda}D_1v_k}\mathbf{a}_k]$.

In the matrix formulation, we have

$$\mathbf{B}_{1,2} = \mathbf{B}_{1,1}\Phi_{v,1}, \quad (12)$$

where $\Phi_{v,1} = \text{diag}[e^{-j\frac{2\pi}{\lambda}D_1v_1}, \dots, e^{-j\frac{2\pi}{\lambda}D_1v_K}]$, and $\text{diag}[\]$ denotes a diagonal matrix with diagonal elements composed of the vector inside $[\]$.

According to the corresponding relationship between the signal subspace and the manifold matrix, we have

$$\mathbf{E}_{s_{1,1}} = \mathbf{B}_{1,1}\mathbf{T}, \quad (13)$$

$$\mathbf{E}_{s_{1,2}} = \mathbf{B}_{1,2}\mathbf{T}, \quad (14)$$

where $\mathbf{E}_{s_{1,1}}$ and $\mathbf{E}_{s_{1,2}}$ are the signal subspace matrices corresponding to $\mathbf{B}_{1,1}$ and $\mathbf{B}_{1,2}$, respectively.

Recalling Eq. (12), we have [28]

$$\mathbf{E}_{s_{1,2}} = \mathbf{E}_{s_{1,1}}\Psi_{v,1}, \quad (15)$$

$$\Psi_{v,1} = \mathbf{T}^{-1}\Phi_{v,1}\mathbf{T}. \quad (16)$$

Theoretically, the k -th eigenvalue of $\Psi_{v,1}$ equals $[\Phi_{v,1}]_{k,k} = e^{-j\frac{2\pi}{\lambda}D_1v_k}$, where $[\]_{m,n}$ extracts (m, n) -th element of the matrix inside $[\]$. Therefore, we perform eigenvalue decomposition to $\Psi_{v,1}$, and the eigenvalues constitutes the estimation of $\Phi_{v,1}$, denoted by $\hat{\Phi}_{v,1}$. Since the inter-sensor spacing D_1 of the sub-array 1 is larger than $\lambda/2$, a high-accuracy but cyclically ambiguous y -axis direction cosine estimation $v_k^{\text{fine},1}$ can be derived by

$$v_k^{\text{fine},1} = -\frac{\angle([\hat{\Phi}_{v,1}]_{k,k})}{2\pi D_1/\lambda}, \quad (17)$$

where \angle denotes the angle of the ensuing entity.

Similarly, from the sub-array 2 with inter-sensor spacing D_2 , we have

$$\mathbf{E}_{s_{2,2}} = \mathbf{E}_{s_{2,1}}\Psi_{v,2}, \quad (18)$$

$$\Psi_{v,2} = \mathbf{T}^{-1}\Phi_{v,2}\mathbf{T}. \quad (19)$$

where $\mathbf{E}_{s_{2,2}}$, $\mathbf{E}_{s_{2,1}}$ and $\Psi_{v,2}$ are calculated from \mathbf{E}_{s_2} .

Similar to Eq. (17), we have

$$v_k^{\text{fine},2} = -\frac{\angle([\hat{\Phi}_{v,2}]_{k,k})}{2\pi D_2/\lambda}. \quad (20)$$

It's worth noting that due to the same column permutation of \mathbf{T} , these two sets of high-accuracy but cyclically ambiguous v estimations are paired automatically [29].

B. VECTOR-CROSS-PRODUCT ALGORITHM TO ESTIMATE U AND UNAMBIGUOUS BUT LOW-ACCURACY V

Based on the above derivation, and due to the relationship between array manifold matrix and signal subspace, we can estimate the manifold matrix of sub-array 1 with

$$\hat{\mathbf{B}}_1 = \mathbf{E}_{s_1} \mathbf{T}^{-1}. \quad (21)$$

Similarly, for the manifold matrix of sub-array 2, we have

$$\hat{\mathbf{B}}_2 = \mathbf{E}_{s_2} \mathbf{T}^{-1}. \quad (22)$$

In order to employ all the SS-EMVSs to perform the vector-cross-product algorithm, we impose a phase compensation and an averaging step to the estimated manifold matrices of the two sub-arrays. According to the principle of ESPRIT algorithm, we know the diagonal elements of $\hat{\Phi}_{v,1}$ are the principle phase differences of different sources resulting from the inter-sensor spacing D_1 of sub-array 1. The sub-array 1 is a uniform linear array (ULA) of SS-EMVS, and the displacement of the n -th ($n = 2, 3, \dots, n_1$) SS-EMVS unit from the first unit is $(n-1)D_1$. Therefore, the phase difference of the n -th unit with the first unit is $\hat{\Phi}_{v,1}^{(n-1)}$. Then the phase difference of the n -th unit in the sub-array 2 with the reference unit is $([\hat{\Phi}_{v,2}]^{n-1}([\hat{\Phi}_{v,1}]^*)^{n-1})$. Thus, employing the diagonal elements of $\hat{\Phi}_{v,1}$ and $\hat{\Phi}_{v,2}$, we can obtain two estimations of the manifold matrix of the reference SS-EMVS, (23) and (24), as shown at the bottom of this page, where the superscript $*$ denotes the conjugate operator, and the “:” represents sequentially picking rows in the matrix.

In other words, for k -th source, we have

$$\hat{\mathbf{q}}_1(k) = c_1 \mathbf{a}_k, \quad \hat{\mathbf{q}}_2(k) = c_2 \mathbf{a}_k, \quad (25)$$

where c_1 and c_2 are two different complex constants [30].

The following is to apply the vector-cross-product algorithm to $\hat{\mathbf{q}}_1(k)$ and $\hat{\mathbf{q}}_2(k)$. For convenience, we omit the source index k , and recalling Eq. (1), where we have $\mathbf{a} = [\tilde{\mathbf{e}}^T, \tilde{\mathbf{h}}^T]^T$ with

$$\tilde{\mathbf{e}} = \begin{bmatrix} e_x \\ e^{-j\frac{2\pi}{\lambda} \Delta_{x,y}} u e_y \\ e^{-j\frac{2\pi}{\lambda} (\Delta_{x,y} + \Delta_{y,z})} u e_z \end{bmatrix}, \quad (26)$$

$$\tilde{\mathbf{h}} = \begin{bmatrix} e^{-j\frac{2\pi}{\lambda} (x_h u + y_h v + z_h w)} h_x \\ e^{-j\frac{2\pi}{\lambda} [(x_h u + y_h v + z_h w) - \Delta_{x,y} u]} h_y \\ e^{-j\frac{2\pi}{\lambda} [(x_h u + y_h v + z_h w) - (\Delta_{x,y} + \Delta_{y,z}) u]} h_z \end{bmatrix}. \quad (27)$$

According to the vector-cross product algorithm [7] of the SS-EMVS, we have,

$$\mathbf{p}_1 = \frac{(c_1 \tilde{\mathbf{e}}) \times (c_1 \tilde{\mathbf{h}})^*}{\|(c_1 \tilde{\mathbf{e}}) \times (c_1 \tilde{\mathbf{h}})^*\|}$$

$$\begin{aligned} &= e^{j\frac{2\pi}{\lambda} (x_h u + y_h v + z_h w)} \begin{bmatrix} u e^{-j\frac{2\pi}{\lambda} (2\Delta_{x,y} + \Delta_{y,z})} u \\ v e^{-j\frac{2\pi}{\lambda} (\Delta_{x,y} + \Delta_{y,z})} u \\ w e^{-j\frac{2\pi}{\lambda} \Delta_{x,y}} u \end{bmatrix} \\ &= \frac{(c_2 \tilde{\mathbf{e}}) \times (c_2 \tilde{\mathbf{h}})^*}{\|(c_2 \tilde{\mathbf{e}}) \times (c_2 \tilde{\mathbf{h}})^*\|} \\ &= \mathbf{p}_2, \end{aligned} \quad (28)$$

where \times denotes the vector-cross product; \mathbf{p}_1 is calculated from $\hat{\mathbf{q}}_1$ and \mathbf{p}_2 is calculated from $\hat{\mathbf{q}}_2$, respectively. Following this, the final vector-cross-product result can be obtained by taking the average, *i.e.*,

$$\mathbf{p} = \frac{\mathbf{p}_1 + \mathbf{p}_2}{2}. \quad (29)$$

From the Poynting vector of k -th source \mathbf{p}_k derived in Eq. (29), we can obtain the *unambiguous but low accuracy* estimations of $\{u_k, v_k, w_k\}$ by

$$\begin{cases} u_k^{\text{coarse}} = |[\mathbf{p}_k]_1|, \\ v_k^{\text{coarse}} = |[\mathbf{p}_k]_2|, \\ w_k^{\text{coarse}} = |[\mathbf{p}_k]_3|, \end{cases} \quad (30)$$

where $[\]_i$ extracts i -th element of the vector inside $[\]$, and $||$ denotes the absolute value of the entity inside $||$. From [30], we know that $\{v_k^{\text{coarse}}\}_{k=1}^K$ and $\{v_k^{\text{fine},1}\}_{k=1}^K$ are paired automatically. And $\{v_k^{\text{fine},1}\}_{k=1}^K$ and $\{v_k^{\text{fine},2}\}_{k=1}^K$ have paired automatically as mentioned above. So till now, $\{v_k^{\text{coarse}}\}_{k=1}^K$, $\{v_k^{\text{fine},1}\}_{k=1}^K$ and $\{v_k^{\text{fine},2}\}_{k=1}^K$ are paired.

In the following, we estimate the high-accuracy estimation of u from the displacement of the dipoles/loops within a single SS-EMVS, *i.e.*, $\Delta_{x,y}$ and $\Delta_{y,z}$ as in [7]. From \mathbf{p} , we can get

$$\mathbf{p}^o = \mathbf{p} \odot e^{-\angle[\mathbf{p}]_1} = \begin{bmatrix} u \\ v e^{j\frac{2\pi}{\lambda} \Delta_{x,y}} u \\ w e^{j\frac{2\pi}{\lambda} (\Delta_{x,y} + \Delta_{y,z})} u \end{bmatrix}, \quad (31)$$

where \odot denotes Hadamard (element-wise) product. Based on Eq. (31), we have two sets of *high-accuracy but cyclically ambiguous* estimations of u by

$$u_k^{\text{fine},1} = \frac{\lambda}{2\pi} \frac{1}{\Delta_{x,y}} \angle \left\{ \frac{[\mathbf{p}_k^o]_2}{v_k^{\text{coarse}}} \right\}, \quad (32)$$

$$u_k^{\text{fine},2} = \frac{\lambda}{2\pi} \frac{1}{\Delta_{x,y} + \Delta_{y,z}} \angle \left\{ \frac{[\mathbf{p}_k^o]_3}{w_k^{\text{coarse}}} \right\}. \quad (33)$$

C. DISAMBIGUATE THE ESTIMATIONS OF U AND V

Due to the fact that there are two sets of high-accuracy but ambiguous estimations for both u and v , a two-order

$$\hat{\mathbf{q}}_1(k) = \frac{\sum_{n=1}^{n_1} \hat{\mathbf{B}}_1 \{[6(n-1)+1] : [6n], k\} ([\hat{\Phi}_{v,1}]_{k,k}^*)^{n-1}}{n_1}, \quad (23)$$

$$\hat{\mathbf{q}}_2(k) = \frac{\sum_{n=1}^{n_2} \hat{\mathbf{B}}_2 \{[6(n-1)+1] : [6n], k\} ([\hat{\Phi}_{v,2}]_{k,k}^*)^{n-1} ([\hat{\Phi}_{v,1}]_{k,k}^*)^{n_1}}{n_2}, \quad (24)$$

disambiguation method is utilized here. We take v as the example to demonstrate the derivation and the process for u is similar [31].

1) DISAMBIGUATE $v_k^{\text{fine},1}$ WITH v_k^{coarse}

The first unambiguous and high-accuracy v estimation can be obtained by

$$v_k^{\text{next}} = v_k^{\text{fine},1} + \hat{m}_1 \frac{\lambda}{D_1}, \quad (34)$$

$$\hat{m}_1 = \underset{m_1}{\operatorname{argmin}} \left| v_k^{\text{coarse}} - v_k^{\text{fine},1} - m_1 \frac{\lambda}{D_1} \right|, \quad (35)$$

where $\lceil (-1 - v_k^{\text{fine},1}) \frac{D_1}{\lambda} \rceil \leq m_1 \leq \lfloor (1 - v_k^{\text{fine},1}) \frac{D_1}{\lambda} \rfloor$ with $\lceil \epsilon \rceil$ denoting the smallest integer not less than ϵ and $\lfloor \epsilon \rfloor$ referring to the largest integer not more than ϵ .

2) DISAMBIGUATE $v_k^{\text{fine},2}$ WITH v_k^{next}

Similarly, we can disambiguate $v_k^{\text{fine},2}$ with v_k^{next} derived above to estimate the final high-accuracy and unambiguous estimation of v :

$$v_k^{\text{final}} = v_k^{\text{fine},2} + \hat{m}_2 \frac{\lambda}{D_2}, \quad (36)$$

$$\hat{m}_2 = \underset{m_2}{\operatorname{argmin}} \left| v_k^{\text{next}} - v_k^{\text{fine},2} - m_2 \frac{\lambda}{D_2} \right|, \quad (37)$$

where $\lceil (-1 - v_k^{\text{fine},2}) \frac{D_2}{\lambda} \rceil \leq m_2 \leq \lfloor (1 - v_k^{\text{fine},2}) \frac{D_2}{\lambda} \rfloor$.

Similar to v , we can obtain the final high-accuracy and unambiguous estimation of u_k^{final} by replacing $\{D_1, D_2\}$ with $\{\Delta_{x,y}, \Delta_{x,y} + \Delta_{y,z}\}$, respectively.

D. ESTIMATING THE DOA AND POLARIZATION PARAMETERS

After getting the unambiguous and high-accuracy estimation of $\{u, v\}$, we can estimate the DOA of k -th source by

$$\begin{cases} \hat{\theta}_k = \arcsin(\sqrt{(u_k^{\text{final}})^2 + (v_k^{\text{final}})^2}), \\ \hat{\phi}_k = \arctan\left(\frac{v_k^{\text{final}}}{u_k^{\text{final}}}\right). \end{cases} \quad (38)$$

Following this, ξ_k in Eq. (1) and $\Theta(\theta_k, \phi_k)$ in Eq. (2) can be estimated, respectively.

Recalling $\hat{q}_1(k), \hat{q}_2(k)$ in Eq. (25) and ξ_k in Eq. (1), a_k^o can be estimated but with a complex constant in the front as

$$\hat{a}_k^o = \hat{q}_1(k) \odot e^{(-\angle \xi_k)} + \hat{q}_2(k) \odot e^{(-\angle \xi_k)}. \quad (39)$$

After this, we can get the estimation of β_k [7]

$$\begin{aligned} \hat{\beta}_k &= \begin{bmatrix} \hat{\beta}_{k,1} \\ \hat{\beta}_{k,2} \end{bmatrix} \\ &= \left[\Theta^H(\hat{\theta}_k, \hat{\phi}_k) \Theta(\hat{\theta}_k, \hat{\phi}_k) \right]^{-1} \Theta^H(\hat{\theta}_k, \hat{\phi}_k) \hat{a}_k^o. \end{aligned} \quad (40)$$

The corresponding polarization parameters $\{\gamma_k, \eta_k\}$ can be estimated by

$$\begin{cases} \hat{\gamma}_k = \arctan \left| \frac{\hat{\beta}_{k,1}}{\hat{\beta}_{k,2}} \right|, \\ \hat{\eta}_k = \angle \frac{\hat{\beta}_{k,1}}{\hat{\beta}_{k,2}}. \end{cases} \quad (41)$$

IV. CRAMÉR-RAO BOUND DERIVATION

A far-field pure-tone with unit-power is used in this section to derive the Cramér-Rao bound (CRB). Given that $s(t) = e^{j(2\pi f_0 t + \epsilon)}$ with a prior-known frequency f_0 and a prior-known initial phase ϵ , with L snapshots uniformly sampled at time-slots $\{t = t_1, t_2, \dots, t_L\}$, we have:

$$s = \left[e^{j(2\pi f_0 t_1 + \epsilon)}, e^{j(2\pi f_0 t_2 + \epsilon)}, \dots, e^{j(2\pi f_0 t_L + \epsilon)} \right]^T. \quad (42)$$

The above sequence is received by the proposed multi-scale SS-EMVS array, corrupted with additive noise $\mathbf{n}(t)$, which is assumed to be zero-mean Gaussian, with its diagonal covariance matrix $\Gamma_0 = \text{diag}[\sigma^2, \dots, \sigma^2]$, where σ^2 refers to the prior-known noise variance at each constituent antenna, $\mathbf{z}(t) = \mathbf{b}s(t) + \mathbf{n}(t)$. The received dataset

$$\begin{aligned} \zeta &= \left[\mathbf{z}^T(t_1), \mathbf{z}^T(t_2), \dots, \mathbf{z}^T(t_L) \right]^T \\ &= \underbrace{\mathbf{s}}_{\text{def } \boldsymbol{\tau}} \otimes \mathbf{b} + \underbrace{\left[\mathbf{n}^T(t_1), \mathbf{n}^T(t_2), \dots, \mathbf{n}^T(t_L) \right]^T}_{\text{def } \mathbf{v}}, \end{aligned} \quad (43)$$

where \mathbf{b} is the array manifold defined in Eq. (4); \mathbf{v} is the noise vector with a covariance matrix $\Gamma = \Gamma_0 \otimes \mathbf{I}_L$, with \mathbf{I}_L denoting an $L \times L$ identity matrix. Hence, ζ is a complex Gaussian distributed process with mean $\boldsymbol{\tau}$ and a covariance matrix Γ . Let

$$\boldsymbol{\psi} \stackrel{\text{def}}{=} [\theta, \phi, \gamma, \eta]^T \quad (44)$$

refer to the vector comprising all the unknown parameters to be estimated. We could derive all the elements of the 4×4 Fisher Information Matrix (FIM) by [32]:

$$J_{[\boldsymbol{\psi}]_i, [\boldsymbol{\psi}]_j} = 2\text{Re} \left[\left(\frac{\partial \boldsymbol{\tau}}{\partial [\boldsymbol{\psi}]_i} \right)^H \Gamma^{-1} \left(\frac{\partial \boldsymbol{\tau}}{\partial [\boldsymbol{\psi}]_j} \right) \right], \quad (45)$$

where $\{J_{[\boldsymbol{\psi}]_i, [\boldsymbol{\psi}]_j}\}_{i,j=1}^4$ refers to the $(i, j)^{\text{th}}$ entry of the FIM, and $\text{Re}[\cdot]$ denotes the real-value part of the entry inside $[\cdot]$. Then the Cramér-Rao bounds of $\boldsymbol{\psi}$ equal:

$$\text{CRB}([\boldsymbol{\psi}]_i) = \left[\mathbf{J}^{-1} \right]_{i,i}, \quad \forall i = 1, 2, 3, 4. \quad (46)$$

The 4×4 Fisher Information Matrix can be expressed as:

$$\mathbf{J} = \begin{bmatrix} J_{\theta,\theta} & J_{\theta,\phi} & J_{\theta,\gamma} & J_{\theta,\eta} \\ J_{\phi,\theta} & J_{\phi,\phi} & J_{\phi,\gamma} & J_{\phi,\eta} \\ J_{\gamma,\theta} & J_{\gamma,\phi} & J_{\gamma,\gamma} & J_{\gamma,\eta} \\ J_{\eta,\theta} & J_{\eta,\phi} & J_{\eta,\gamma} & J_{\eta,\eta} \end{bmatrix}. \quad (47)$$

The Cramér-Rao bounds for each parameter can be obtained straightforwardly from Eq. (46) after we get the values of \mathbf{J} by Eq. (45).¹

¹For the Gaussian source scenario, please refer to the derivation in [33].

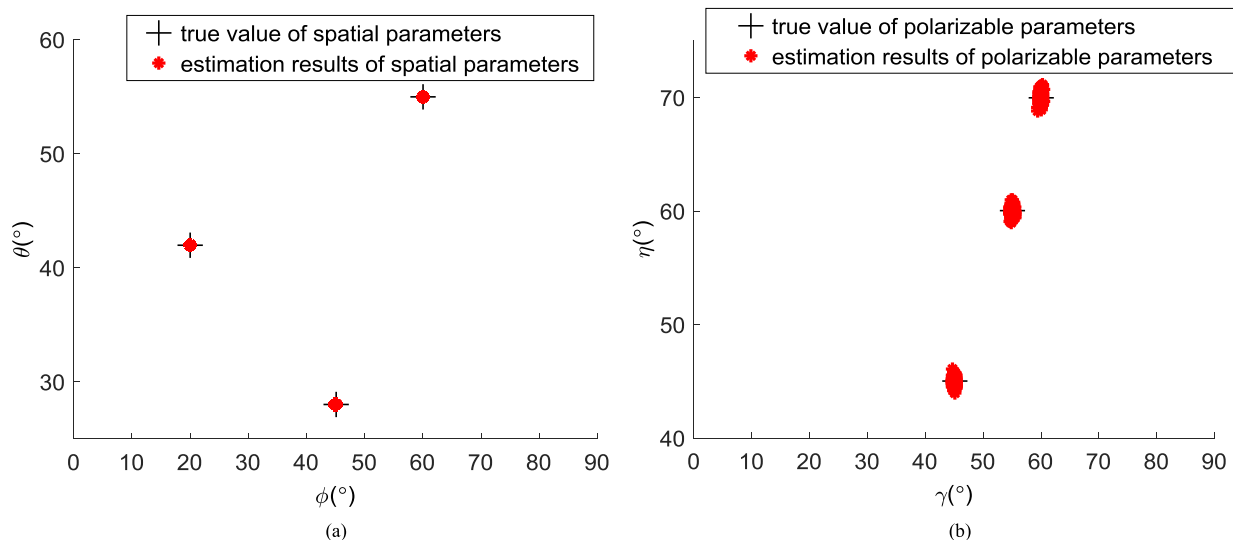


FIGURE 3. The estimation results of three incident sources: (a) spatial parameters, and (b) polarization parameters.

V. SIMULATION RESULTS

In this section, we conduct simulations to verify the effectiveness and performance of the proposed array geometry and algorithm. For simplicity, we set $\theta \in [0, \pi/2]$, $\phi \in [0, \pi)$. The coordinate of the h_x of the reference SS-EMVS, whose e_x is located at the origin, is $(x_h, y_h, z_h) = (7.5\lambda, 5\lambda, 10\lambda)$. The root mean square error (RMSE) of parameter estimation is defined as:

$$RMSE = \sqrt{\frac{1}{M} \sum_{m=1}^M (\hat{\alpha}_m - \alpha)^2}, \quad (48)$$

where $\hat{\alpha}_m$ is the estimation of m -th trial of parameter α , and M is the number of Monte Carlo trials. We assume that the number of sources is known a priori in the following simulations.

A. PARAMETER ESTIMATION RESULTS

In the first example, we consider that there are $N = 10$ SS-EMVSs placed along the y -axis direction. The first five SS-EMVSs compose the sub-array 1 with inter-sensor spacing $D_1 = 6\lambda$; the rest SS-EMVSs constitute the sub-array 2 with inter-sensor spacing $D_2 = 6D_1 = 36\lambda$. For every SS-EMVS, $\Delta_{x,y} = \Delta_{y,z} = 5\lambda$. There are $K = 3$ single-frequency incident sources with unit power, which have the numerical frequency $f = (0.537, 0.233, 0.277)$, elevation $\theta = (20^{\circ}, 60^{\circ}, 45^{\circ})$, azimuth $\phi = (42^{\circ}, 55^{\circ}, 28^{\circ})$, the auxiliary polarization angle $\gamma = (45^{\circ}, 60^{\circ}, 55^{\circ})$, and the polarization phase difference $\eta = (45^{\circ}, 70^{\circ}, 60^{\circ})$ impinging on the array. The number of snapshots is $L = 200$ and SNR=15dB. The noise is complex Gaussian white noise vector with zero mean and covariance matrix $\sigma^2\mathbf{I}$. Fig. 3 shows the estimation results of the proposed algorithm with 200 Monte Carlo trials. We can see that the spatial and polarization parameters of all targets are correctly paired and estimated.

B. PARAMETER ESTIMATION PERFORMANCE

In order to further exploit the performance of the proposed array, we hereby conduct various simulations with different parameters of the array and sources. Since our sparse array in Fig. 2 extends the aperture along the y -axis, we focus on the analysis of the v estimation below. Two similar arrays, which extend the aperture along the x -axis and the z -axis respectively, will be analyzed at the end of this section.

1) PERFORMANCE VERSUS SNR

In the second example, we consider the parameter estimation performance versus SNR (signal-to-noise ratio). Fig. 4(a) shows the RMSE of u^{final} of the proposed array versus SNR compared with u^{coarse} and the CRB. Fig. 4(b) shows the RMSE of v^{next} and v^{final} of the proposed array versus SNR compared with v^{coarse} and the CRB. It can be observed that both u^{final} and v^{final} improve significantly from their coarse estimates, u^{coarse} and v^{coarse} , respectively; both of them are getting close to their CRB. We can also see that the estimation performance of v^{final} is an order of magnitude better than that of u^{final} . The reason is that the proposed array only extends in the y -axis (up to 174λ), while the accuracy of u^{final} is limited by the expansion of the single SS-EMVS in the x -axis, which is only 10λ .

Next, we compare the proposed multiscale SS-EMVS array with two uniform SS-EMVS arrays, and both of them have the same number of SS-EMVSs, but with inter-sensor spacing $d_1 = D_1 = 6\lambda$ and $d_2 = D_2 = 36\lambda$, respectively. These two arrays are one type of the sparse polarized antenna arrays proposed in [10], for which only a single disambiguation step is required since it is a uniform array along y -axis. By contrast, our proposed array is a multiscale array and thus can provide better performance. Fig. 5 shows the RMSE of u and v estimations versus SNR for all three sparse arrays. We understand that there is a SNR threshold [34] in

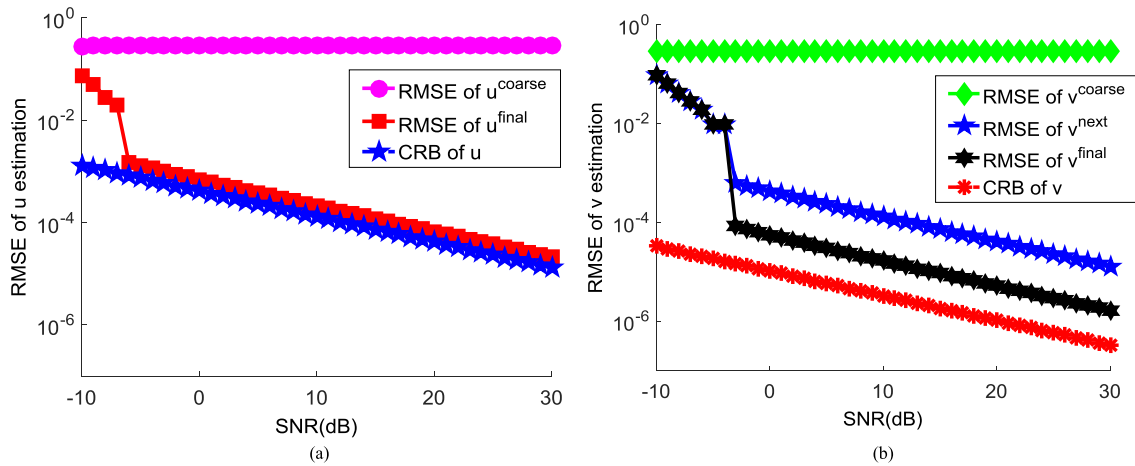


FIGURE 4. The RMSE of (a) u^{coarse}, u^{final} compared with CRB, and (b) v^{coarse}, v^{next} and v^{final} compared with CRB using the proposed array.

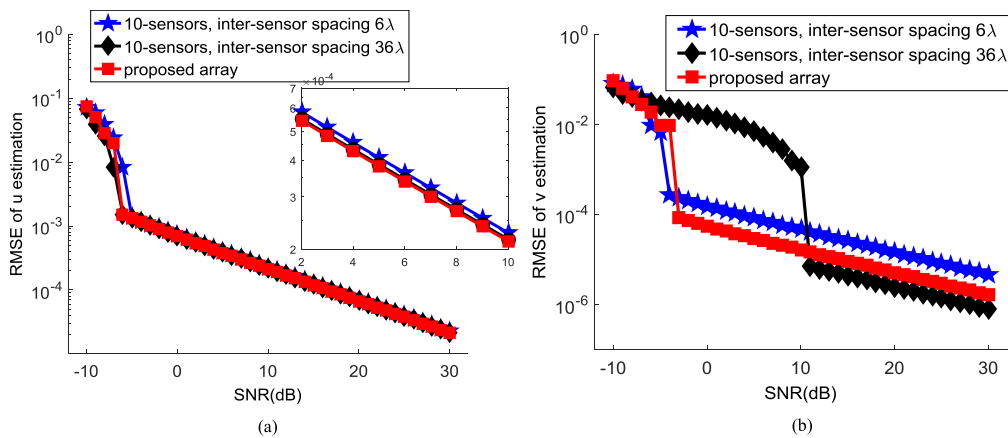


FIGURE 5. RMSE of u and v estimations of the proposed array and two uniform SS-EMVS arrays (with inter-sensor spacing 6λ and 36λ , respectively) versus SNR. (a) RMSE of u estimation, and (b) RMSE of v estimation.

the process of disambiguation. The parameter estimation performance will be degraded significantly if the SNR is lower than the threshold. When SNR is larger than this threshold, the performance improves dramatically, and the performance is getting better with the increase of SNR. We can observe from Fig. 5(a) that the performances of these three arrays of the u estimation are similar. This is because the three arrays have the same extension in the x -axis. But the accuracy of the proposed array of u estimation is merely a little better than the two other arrays when SNR is large enough, *i.e.*, > -6 dB. More importantly, from Fig. 5(b), we can observe that the SNR threshold (-3 dB) of v estimation of the proposed array is close to the threshold (-4 dB) of the uniform SS-EMVS array whose inter-sensor spacing is d_1 and is far less than that (11 dB) of the uniform SS-EMVS array whose inter-sensor spacing is d_2 . Limited by the array aperture in the y -axis, the accuracy of the proposed array of v estimation is in between of these two uniform SS-EMVS arrays.

As the arriving angle estimation is determined by u and v jointly, in Fig. 6, we plot the RMSE of the estimated θ and ϕ of the three arrays versus SNR. It can be seen that

the estimation accuracies of θ or ϕ of the three arrays are similar when SNR is large enough, *i.e.*, > 10 dB. But we still can see that the accuracy of θ and ϕ of the proposed array is a little (0.01°) better than the two other arrays. Compared with the SS-EMVS array whose inter-sensor spacing is d_1 , the proposed array has a larger aperture and a better accuracy estimation. The inter-sensor spacing is larger than d_1 in sub-array 2 and thus the mutual coupling is reduced. Furthermore, the threshold of the proposed array is far (11 dB) smaller than that of the SS-EMVS array with inter-sensor spacing d_2 . Therefore, our proposed array is a good trade-off of mutual coupling, estimation accuracy, and robustness (lower SNR threshold) to noise.

2) PARAMETER v ESTIMATION PERFORMANCE VERSUS SNAPSHOT NUMBER

In the next example, we consider the performance of v estimation with the collected snapshot L , to verify the performance of the proposed array in limited time. Fig. 7 shows the RMSE of v estimation of the three arrays versus L at SNR = 10 dB. We can see that the v estimation performance of the proposed

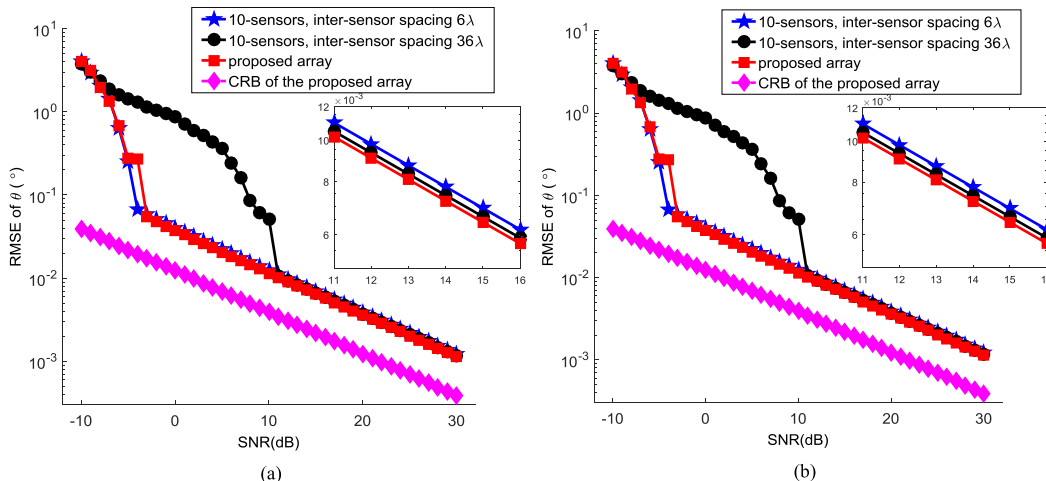


FIGURE 6. RMSE of θ and ϕ estimation of the three arrays versus SNR. (a) RMSE of θ estimation, and (b) RMSE of ϕ estimation.

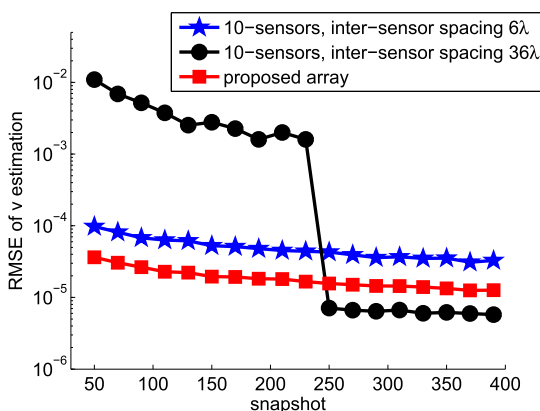


FIGURE 7. RMSE of v estimation of the three arrays versus snapshot.

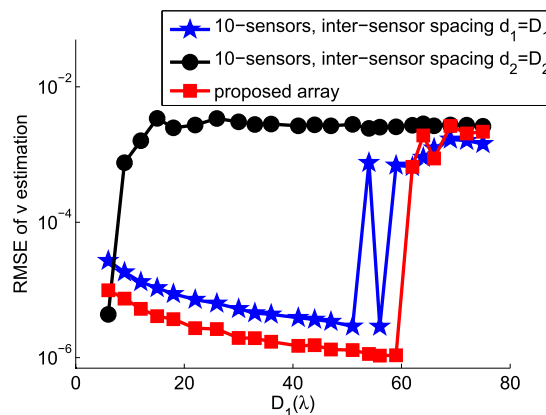


FIGURE 8. RMSE of v estimation of the three arrays versus D_1 .

array improves with the increase of snapshots. Limited by the array aperture in the y -axis, the accuracy of the proposed array of v estimation is in between of the two uniform SS-EMVS arrays, when L is large enough, *i.e.* > 250 . Unfortunately, when the snapshot is small, *i.e.*, < 230 , the uniform array with larger inter-sensor spacing d_2 provides the worst estimation performance of v . By contrast, our proposed array consistently provides good estimations.

3) PARAMETER v ESTIMATION PERFORMANCE VERSUS D_1

Besides, we consider the performance variation of v estimation with the first sub-array inter-sensor spacing D_1 , and again we set $D_2 = 6D_1$, $d_1 = D_1$, $d_2 = D_2$. We know that larger inter-sensor spacing will lead to larger aperture, and thus better estimation performance. However, this will introduce challenge to the disambiguation. Therefore, there is a baseline length threshold [35] in the process of disambiguation. When the inter-sensor spacing value becomes larger than threshold, the disambiguation process will break down. Fig. 8 plots the RMSE of v estimation of the three arrays versus D_1 at

SNR = 15dB. We can see that the baseline length threshold of the proposed array (60λ) is larger than the two other arrays (8λ , 55λ) because of the proposed two order disambiguation. Moreover, the accuracy of the v estimation of the proposed array is better than those of the two other arrays when the D_1 value is smaller than the threshold.

C. PARAMETER ESTIMATION RESULTS OF COHERENT SIGNALS

For coherent signals, the proposed algorithm is still effective by adding an extra spatial-smoothing step [10] before the ESPRIT based method developed in Section III-A. We consider $K = 3$ unit power sources with the same numerical frequency $f = (0.537, 0.537, 0.537)$. Other source and simulation parameters keep the same as those in Section V-A. Fig. 9 shows the estimation results with 200 Monte Carlo trials. We can see that the spatial and polarization parameters of all coherent sources are correctly paired and estimated. This demonstrates the effectiveness of our estimation algorithm to coherent signals.

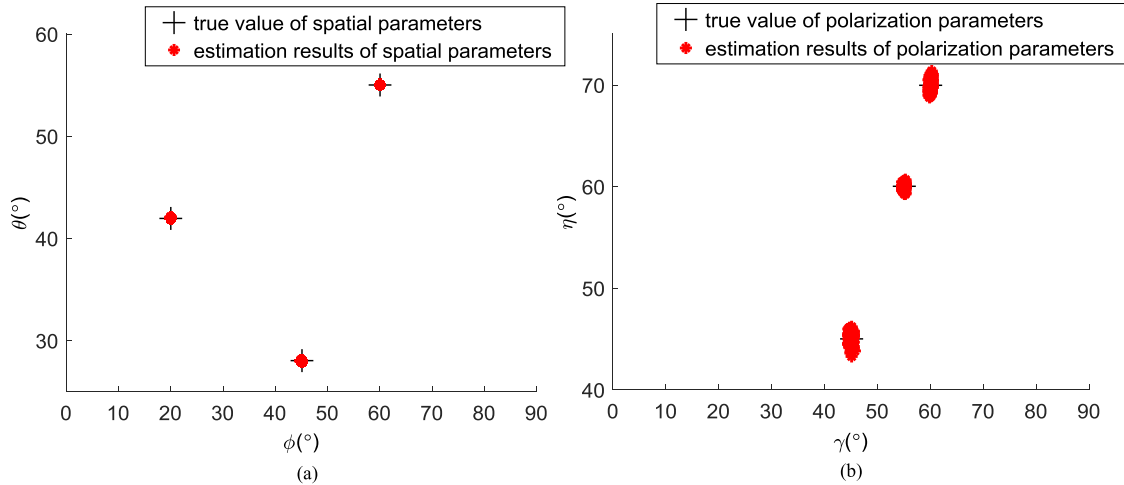


FIGURE 9. The estimation results of three coherent incident sources: (a) spatial parameters, and (b) polarization parameters.

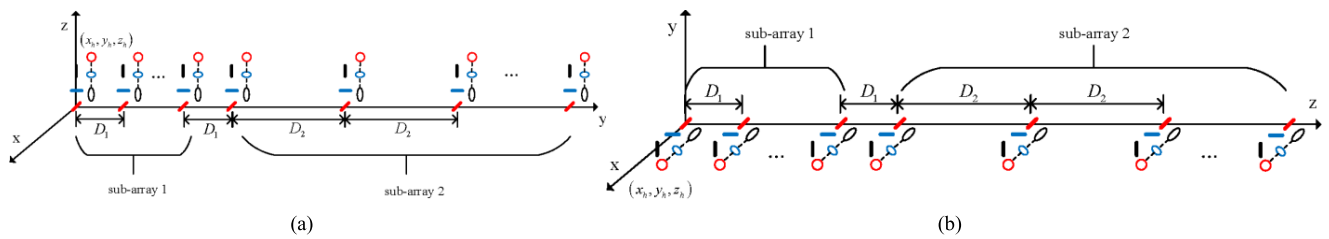


FIGURE 10. The two other array geometries. (a) y-axis extension and each SS-EMVS is parallel to z-axis, and (b) z-axis extension and each SS-EMVS is parallel to x-axis.

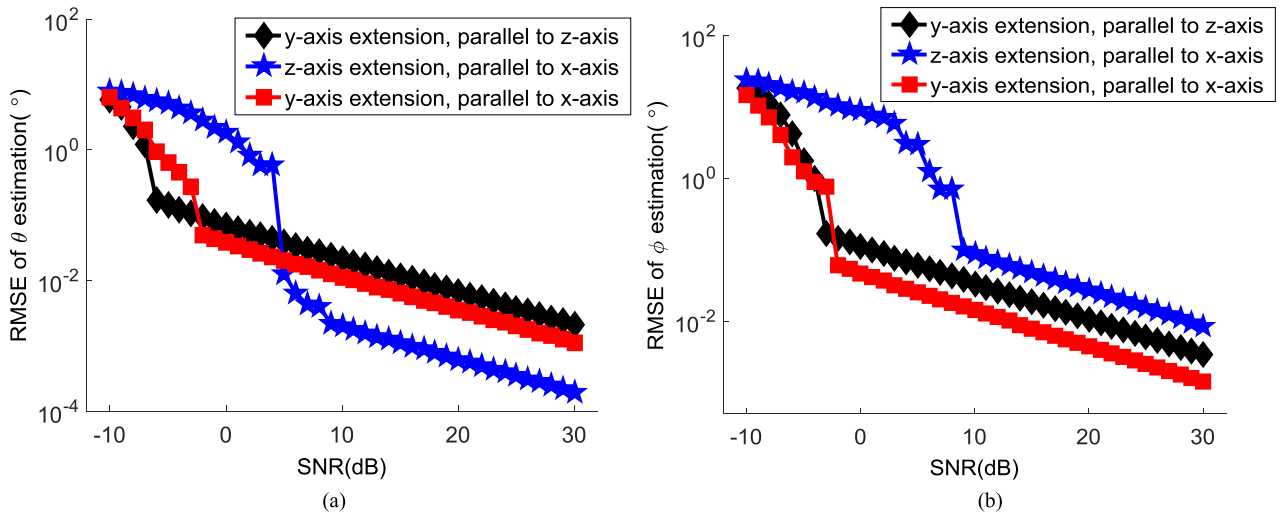


FIGURE 11. RMSE of θ and ϕ estimation of the three array geometries in Fig. 2 and Fig. 10. (a) RMSE of θ estimation, and (b) RMSE of ϕ estimation.

D. DOA ESTIMATION PERFORMANCE OF DIFFERENT ARRAY CONFIGURATIONS

As mentioned earlier, we now consider different arrangements of the SS-EMVS array. Specifically, we discuss two other array configurations. The first one is that the array is extended along y-axis and every SS-EMVS is parallel to z-axis direction; the second one is that the array is extended

along z-axis and every SS-EMVS is parallel to x-axis direction. Fig. 10 depicts these two array geometries. Using the same simulation parameters as in Section V-A, we compare the angle estimation performance of these two arrays and the proposed array shown in Fig. 2. The results are given in Fig. 11. We can observe that the second array configuration has a better performance in θ estimation, which is reasonable

as the estimation accuracy of the θ mainly depends on the z -axis aperture and the second array has the largest z -axis extension. Unfortunately, the SNR threshold of this array (5dB) is significantly larger than two other arrays (-6dB, -2dB) and the performance in azimuth dimension is the worst. Therefore, taking a comprehensive consideration, the array configuration, in which the array is parallel to y -axis and each SS-EMVS is parallel to x -axis direction, is the optimum choice for our applications.

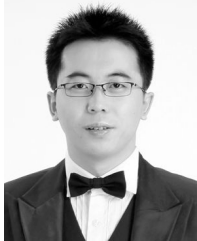
VI. CONCLUSIONS

In this paper, a multiscale spatially-spread electromagnetic-vector-sensor array is proposed, which enjoys the superiorities of the spatially-spread electromagnetic-vector-sensor and the sparse array. Based on this, a new algorithm for direction-of-arrival and polarization parameters estimation has been developed. The proposed algorithm utilizes the approach of two order disambiguation. Via comparing with uniform linear arrays composed of the same number of spatially spread electromagnetic vector-sensors, we have demonstrated that our proposed array geometries enjoy the optimal trade-off on estimation accuracy, mutual coupling and robustness to noise. Theoretically, our proposed array can have as many scales *i.e.*, sub-arrays, as possible, and the algorithm framework can be used straightforwardly. More scales will lead to better estimation performance, but with more sensors and cost. Therefore, it is always a trade-off between cost and performance. We believe that our proposed array geometries give some new breath to engineers in array design.

REFERENCES

- [1] K. T. Wong and M. D. Zoltowski, "Uni-vector-sensor ESPRIT for multi-source azimuth, elevation, and polarization estimation," *IEEE Trans. Antennas Propag.*, vol. 45, no. 10, pp. 1467–1474, Oct. 1997.
- [2] A. Nehorai and P. Tichavsky, "Cross-product algorithms for source tracking using an EM vector sensor," *IEEE Trans. Signal Process.*, vol. 47, no. 10, pp. 2863–2867, Oct. 1999.
- [3] L. Sun, G. Ou, and Y. Lu, "Vector sensor cross-product for direction of arrival estimation," in *Proc. 2nd Int. Congr. Image Signal Process. (CISP)*, Oct. 2009, pp. 1–5.
- [4] K. T. Wong and M. D. Zoltowski, "Closed-form direction finding and polarization estimation with arbitrarily spaced electromagnetic vector-sensors at unknown locations," *IEEE Trans. Antennas Propag.*, vol. 48, no. 5, pp. 671–681, May 2000.
- [5] Y. G. Xu and Z. W. Liu, "Regularized ESPRIT-based direction finding and polarization estimation with one electromagnetic vector sensor," in *Proc. 7th Int. Conf. Signal Process. (ICSP)*, vol. 1, Aug. 2004, pp. 399–402.
- [6] X. Yuan, "Estimating the DOA and the polarization of a polynomial-phase signal using a single polarized vector-sensor," *IEEE Trans. Signal Process.*, vol. 60, no. 3, pp. 1270–1282, Mar. 2012.
- [7] K. T. Wong and X. Yuan, "'Vector cross-product direction-finding' with an electromagnetic vector-sensor of six orthogonally oriented but spatially noncollocating dipoles/loops," *IEEE Trans. Signal Process.*, vol. 59, no. 1, pp. 160–171, Jan. 2011.
- [8] F. Luo and X. Yuan, "Enhanced 'vector-cross-product' direction-finding using a constrained sparse triangular-array," *EURASIP J. Adv. Signal Process.*, vol. 2012, p. 115, Dec. 2012, doi: [10.1186/1687-6180-2012-115](https://doi.org/10.1186/1687-6180-2012-115).
- [9] Y. Li and J. Q. Zhang, "An Enumerative NonLinear Programming approach to direction finding with a general spatially spread electromagnetic vector sensor array," *Signal Process.*, vol. 93, no. 4, pp. 856–865, 2013.
- [10] X. Yuan, "Coherent sources direction finding and polarization estimation with various compositions of spatially spread polarized antenna arrays," *Signal Process.*, vol. 102, pp. 265–281, Sep. 2014.
- [11] J. He and Z. Liu, "Computationally efficient 2D direction finding and polarization estimation with arbitrarily spaced electromagnetic vector sensors at unknown locations using the propagator method," *Digit. Signal Process.*, vol. 19, no. 3, pp. 491–503, 2009.
- [12] X. Yuan, "Spatially spread dipole/loop quads/quints: For direction finding and polarization estimation," *IEEE Antennas Wireless Propag. Lett.*, vol. 12, pp. 1081–1084, 2013.
- [13] L. Wang, Z. Chen, G. Wang, and X. Rao, "Estimating DOA and polarization with spatially spread loop and dipole pair array," *J. Syst. Eng. Electron.*, vol. 26, no. 1, pp. 44–49, 2015.
- [14] X. Zhang, Z. Liu, W. Liu, and Y. Xu, "Quasi-vector-cross-product based direction finding algorithm with a spatially stretched tripole," in *Proc. IEEE Region Conf. (TENCON)*, Oct. 2013, pp. 1–4.
- [15] K. T. Wong and M. D. Zoltowski, "Sparse array aperture extension with dual-size spatial invariances for ESPRIT-based direction finding," in *Proc. IEEE 39th Midwest Symp. Circuits Syst.*, vol. 2, Aug. 1996, pp. 691–694.
- [16] V. I. Vasylyshyn, "Unitary ESPRIT-based DOA estimation using sparse linear dual size spatial invariance array," in *Proc. Eur. Radar Conf. (EURAD)*, Oct. 2005, pp. 157–160.
- [17] A. L. Swindlehurst, B. Ottersten, R. Roy, and T. Kailath, "Multiple invariance ESPRIT," *IEEE Trans. Signal Process.*, vol. 40, no. 4, pp. 867–881, Apr. 1992.
- [18] A. Moffet, "Minimum-redundancy linear arrays," *IEEE Trans. Antennas Propag.*, vol. AP-16, no. 2, pp. 172–175, Mar. 1968.
- [19] P. Pal and P. P. Vaidyanathan, "Nested arrays: A novel approach to array processing with enhanced degrees of freedom," *IEEE Trans. Signal Process.*, vol. 58, no. 8, pp. 4167–4181, Aug. 2010.
- [20] P. P. Vaidyanathan and P. Pal, "Sparse sensing with co-prime samplers and arrays," *IEEE Trans. Signal Process.*, vol. 59, no. 2, pp. 573–586, Feb. 2011.
- [21] X. Shi and Y. Wang, "Parameter estimation of distributed sources with electromagnetic vector sensors," in *Proc. 9th Int. Conf. Signal Process. (ICSP)*, Oct. 2008, pp. 203–206.
- [22] X. Gong, Z. Liu, and Y. Xu, "Quad-quaternion MUSIC for DOA estimation using electromagnetic vector sensors," *EURASIP J. Adv. Signal Process.*, vol. 2008, no. 1, p. 213293, Dec. 2009.
- [23] M. Diao and C. An, "Direction finding of coexisted independent and coherent signals using electromagnetic vector sensor," *J. Syst. Eng. Electron.*, vol. 23, no. 4, pp. 481–487, Aug. 2012.
- [24] K. Han and A. Nehorai, "Nested vector-sensor array processing via tensor modeling," *IEEE Trans. Signal Process.*, vol. 62, no. 10, pp. 2542–2553, May 2014.
- [25] J. He, Z. Zhang, T. Shu, and W. Yu, "Direction finding of multiple partially polarized signals with a nested cross-dipole array," *IEEE Antennas Wireless Propag. Lett.*, vol. 16, pp. 1679–1682, 2017.
- [26] S. Rao, S. P. Chepuri, and G. Leus, "DOA estimation using sparse vector sensor arrays," in *Proc. IEEE 6th Int. Workshop Comput. Adv. Multi-Sensor Adapt. Process. (CAMSAP)*, Dec. 2015, pp. 333–336.
- [27] R. Roy and T. Kailath, "Esprit-estimation of signal parameters via rotational invariance techniques," *IEEE Trans. Acoust., Speech, Signal Process.*, vol. 37, no. 7, pp. 984–995, Jul. 1989.
- [28] C. Jinli, G. Hong, and S. Weimin, "Angle estimation using ESPRIT without pairing in MIMO radar," *Electron. Lett.*, vol. 44, no. 24, pp. 1422–1423, Nov. 2008.
- [29] J. Li, M. Shen, and D. Jiang, "DOA estimation based on combined ESPRIT for co-prime array," in *Proc. IEEE 5th Asia-Pacific Conf. Antennas Propag. (APCAP)*, Jul. 2016, pp. 117–118.
- [30] G. Zheng, B. Wu, Y. Ma, and B. Chen, "Direction of arrival estimation with a sparse uniform array of orthogonally oriented and spatially separated dipole-triads," *IET Radar, Sonar Navigat.*, vol. 8, no. 8, pp. 885–894, Oct. 2014.
- [31] V. I. Vasylyshyn, "Closed-form DOA estimation with multiscale unitary ESPRIT algorithm," in *Proc. 1st Eur. Radar Conf. (EURAD)*, 2004, pp. 317–320.
- [32] H. L. Van Trees, *Optimum Array Processing: Part IV of Detection, Estimation, and Modulation Theory*. New York, NY, USA: Wiley, 2002.
- [33] X. Yuan, "Cramer-Rao bounds of direction-of-arrival and distance estimation of a near-field incident source for an acoustic vector sensor: Gaussian source and polynomial-phase source," *IET Radar, Sonar Navigat.*, vol. 6, no. 7, pp. 638–648, 2012.

- [34] C. D. Richmond, "Mean-squared error and threshold SNR prediction of maximum-likelihood signal parameter estimation with estimated colored noise covariances," *IEEE Trans. Inf. Theory*, vol. 52, no. 5, pp. 2146–2164, May 2006.
- [35] F. Athley, "Threshold region performance of maximum likelihood direction of arrival estimators," *IEEE Trans. Signal Process.*, vol. 53, no. 4, pp. 1359–1373, Apr. 2005.



MINGLEI YANG (M'14) received the B.E. degree in electronic engineering and the Ph.D. degree from Xidian University, China, in 2004 and 2009, respectively. Since 2009, he has been with the National Laboratory of Radar Signal Processing, Xidian University, where he is currently an Associate Professor.

From 2014 to 2015, he was a Visiting Scholar with the Elisha Yegal Bar-Ness Center for Wireless Communications and Signal Processing Research, New Jersey Institute of Technology. He has been doing research in the fields of array signal processing, MIMO signal processing, and polarization information processing. He has published over 60 peer-reviewed journals and conference papers and over 40 inventions.



JIN DING received the B.E. degree in electronic information engineering from the Harbin Institute of Technology, Weihai, China, in 2016. He is currently pursuing the master's degree with the National Laboratory of Radar Signal Processing, Xidian University. His research interests include radar signal processing and array signal processing.



BAIXIAO CHEN was born in Anhui, China, in 1966. He received the degree from the Metallurgy College of East China in 1987, and the master's degree in circuit and system and the Ph.D. degree in signal and information processing from Xidian University, in 1994 and 1997, respectively. He was with the Metallurgy College of East China from 1987 to 1991. Since 1997, he has been a Faculty Member with the National Laboratory of Radar Signal Processing. He was a Lecturer from 1997 to 1999 and an Associate Professor from 1996 to 2003. In 2006, he was selected into the New Century Elitist Support Program of the Ministry of Education. He is currently a Professor in signal and information processing. His general research interests include radar signal processing, new radar system design, array signal processing, and precise guidance.



XIN YUAN (S'09–M'12–SM'16) received the B.Eng. and M.Eng. degrees from Xidian University, in 2007 and 2009, respectively, and the Ph.D. degree from the Hong Kong Polytechnic University, in 2012.

From 2012 to 2015, he was a Post-Doctoral Associate with the Department of Electrical and Computer Engineering, Duke University. Since 2015, he has been a Video Analysis and Coding Lead Researcher with the Nokia Bell Labs, Murray Hill, NJ, USA. He has authored two book chapters, over 70 articles, and over 10 inventions. His research interests include signal processing, computational photography, image processing, machine learning, and computer vision. He develops compressive sensing techniques for high-dimensional imaging with applications to videos, hyperspectral, microscopy, and X-ray images.

Two papers he co-authored won the best paper award in the Computational Optical Sensing and Imaging Conferences, in 2013 and 2014, on video compressive sensing and on depth compressive sensing cameras, respectively.

...